BL4B

Collective Auger Decay of Double Inner-Shell Vacancies in Xe Studied by Multielectron–Ion Coincidence Spectroscopy

Y. Hikosaka[1]

[1]*Institute of Liberal Arts and Sciences, University of Toyama, Toyama 930-0194, Japan*

Auger decay of atomic and molecular core holes generally involves two-electron transitions, where an electron fills an inner-shell vacancy, causing another electron to be emitted into the continuum. An uncommon Auger process, called cascade Auger decay (CAD), can occur when double inner-shell vacancies form in atoms and molecules. Here, two outer electrons simultaneously fill the double vacancies while releasing a single high-energy Auger electron. This study investigates the CAD of Xe^{2+} $4d^{-2}$ double core-hole states using multielectron–ion coincidence spectroscopy with a magnetic bottle electron spectrometer [1,2]. Its high coincidence efficiency allows a detailed spectroscopic analysis of the very rare decay path of double core-hole states.

Figure 1(a) presents an Auger spectrum coincident with a $3d_{5/2}$ photoelectron, measured at a photon energy of 921.2 eV. The formation of $4d^{-2}$ double core-hole states is most prominent among the first-step Auger transitions from the $3d_{5/2}^{-1}$ state. The yields recorded in further coincidence with Xe^{3+} and Xe^{4+} are shown in red and blue, respectively, with ion detection efficiency being compensated. The decay of the double core-hole states mainly results in the production of Xe^{4+} due to cascade double Auger decay. Meanwhile, the red spectrum manifests that the decay of the $4d^{-2}$ states weakly produces Xe^{3+} through the emission of a single Auger electron, indicating a CAD path.

The Xe^{3+} levels populated by the CAD are distinctly observable in the single Auger electron spectrum emitted from the $4d^{-2}$ states. The Auger electron should be detected in a four-fold coincidence with a 3d photoelectron, an $M_{4,5}N_{4,5}N_{4,5}$ Auger electron, and a Xe^{3+} ion. The single Auger electron spectrum extracted is shown in Fig. 1(b), where the Auger transition energies from Xe^{2+} $4d^{-2}$ to Xe^{3+} $5l^{-3}$ levels and the energy position of the Xe^{4+} threshold relative to Xe^{2+} $4d^{-2}$ are indicated. The spectrum exhibits a broad structure in the kinetic energy range of 45–100 eV, suggesting that excited Xe^{3+} levels up to the Xe^{4+} threshold are predominantly produced by the CAD. This spectral feature differs significantly from the CAD observation for Ar^{2+} $2p^{-2}$, where Ar^{3+} $3p^{-3}$ ground states are mainly produced [3].

Peculiar behavior in the CAD of Xe^{2+} $4d^{-2}$ levels is observed also in the branching ratio relative to the total decay of the double core-hole states. The branching ratio is estimated from the coincidence yields to be as large as $2 \times 10^{-2} \pm 1 \times 10^{-2}$. The CAD branching ratio for Ar^{2+} $2p^{-2}$ states was reported to be $1.9 \times 10^{-3} \pm 1.0 \times 10^{-3}$ experimentally and approximately 1.0×10^{-3} theoretically [3]. Thus, the CAD branching ratio for Xe^{2+} $4d^{-2}$ double core-hole states is an order of magnitude greater than that for Ar^{2+} $2p^{-2}$. This amplified CAD for Xe^{2+} $4d^{-2}$, along with the favorable formation of excited Xe^{3+} levels, can be explained by analyzing the number and locations of intermediate configurations needed to promote CAD in second-order perturbation theory [4].

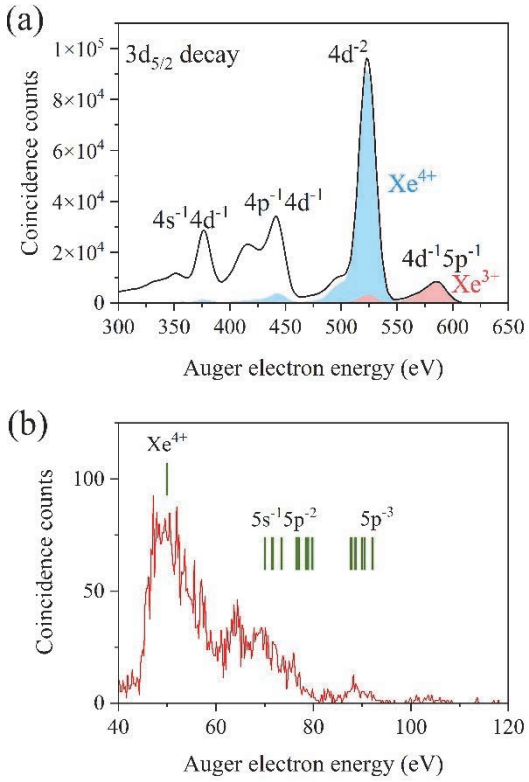

Fig. 1. (a) Coincident Auger spectrum (black) associated with the $3d_{5/2}$ core-hole state of Xe. The yield of Auger electrons, filtered further in coincidence with the Xe^{3+} and Xe^{4+} product ions, are shown in red and blue shading, respectively. (b) Spectrum of single Auger electrons emitted from the Xe^{2+} $4d^{-2}$ states populated via the decay of the $3d_{5/2}$ single vacancy levels, obtained through four-fold coincidence with a 3d photoelectron, an $M_{4,5}N_{4,5}N_{4,5}$ Auger electron, and a Xe^{3+} ion.

[1] Y. Hikosaka and E. Shigemasa, Int. J. Mass Spectrom. **439** (2019) 13.
[2] Y, Hikosaka, J. Electron Spectrosc. Relat. Phenom. **255** (2022) 147158.
[3] M. Mailhiot *et al*., Phys. Rev. A **107** (2023) 063108.
[4] Y. Hikosaka and S. Fritzsche, Phys. Rev. Lett. **134** (2025) 103001.

BL4B

Soft X-ray Absorption Study of Semiconductor Photocatalysts Excited with Steady UV Light

Y. H. Chew[1], H. Onishi[1,2], N. Ichikuni[3] and T. Yoshida[4]
[1]*School of Science, Kobe University, Kobe 657-8501, Japan*
[2]*Division of Advanced Molecular Science, Institute for Molecular Science, Okazaki 444-8585, Japan*
[3]*Graduate School of Engineering, Chiba University, Chiba 263-8522, Japan*
[4]*Graduate School of Engineering, Nagoya University, Nagoya 464-8603, Japan*

Materials conversion on semiconductor photocatalysts has been intensively studied worldwide. Downhill reactions, in which the Gibbs free energy decreases during the conversion of reactants to products, have been successfully integrated into our society [1]. Artificial photosynthesis, a category of uphill reactions involving the oxidation of water, is being developed for societal implementation in the near future [2]. In addition, fundamental studies are being conducted to uncover new scientific discoveries related to light-driven, efficient materials conversion.

Here, in collaboration with Prof. Hiroshi Iwayama of UVSOR, we apply soft X-ray absorption to the characterization of semiconductor photocatalysts under UV light irradiation for band-gap excitation. A series of metal oxide photocatalysts including sodium tantalate ($NaTaO_3$), strontium titanate ($SrTiO_3$), titanium oxide (TiO_2), tin oxide (SnO_2), and zinc oxide (ZnO) were investigated in a beam time in FY2024.

The photocatalyst particles were formed into disks of 7 mm diameter. The disks were placed in a vacuum chamber, irradiated with incident X-rays, and the fluorescent X-rays were detected with a silicon drift detector (SDD). The detector was capped with a 150 nm thick aluminum film (LUXEL, TF110) to minimize the contribution of stray UV light to the detector response (Fig. 1). The capping device is deposited at UVSOR. Users are encouraged to use the device when operating the SDD under UV or visible light irradiation.

Figure 2 shows a set of fluorescence yield spectra at the oxygen K-edge observed on a $NaTaO_3$ photocatalyst doped with Sr^{2+} cations, in the presence and absence of UV light provided by a Hg–Xe lamp (200 W).

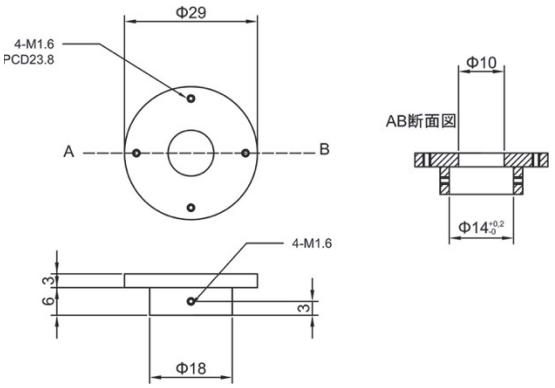

Fig. 1. A devise capping the SDD with the aluminum filter for fluorescence yield detection of oxygen K edge absorption spectrum under UV-light irradiation.

In the oxygen K-edge, electron transition from O1s to O2p orbitals of $NaTaO_3$ particles was detected. The O2p orbitals are hybridized with Ta5d orbitals to form the conduction band in perovskite-structured $NaTaO_3$. The hybridized O2p orbitals are thus split into t_{2g} and e_g levels, one at 532.6 eV and the other at 537.7 eV, according to the ligand field in TaO_6 octahedra.

The t_{2g} and e_g bands shifted to the low energy side under UV irradiation. The shifted bands induced differentiated forms in the difference spectrum. A possible reason for the band shifts is the conduction band partially filled with electrons excited across the band gap, where the oxidation state of some Ta cations decreased from 5+ to 4+.

The X-ray absorption of electronically excited metal oxides has been studied using ultrashort light pulses [3]. Here, we showed that the absorption spectrum was also sensitive to steady light irradiation. This study was supported by JSPS KAKENHI (grant number 22H00344).

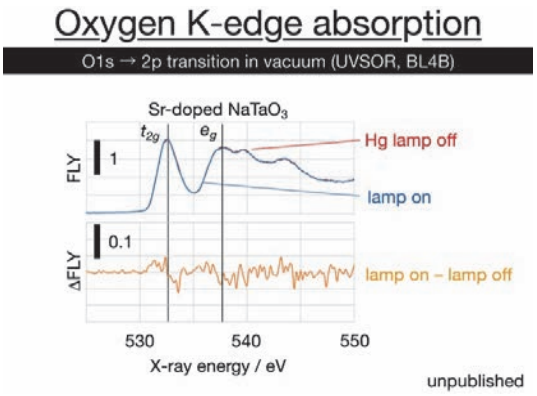

Fig. 2. Oxygen K edge absorption spectrum of a $NaTaO_3$ photocatalyst doped with Sr^{2+} cations in the absence (red spectrum) and presence (blue spectrum) of UV irradiation. The difference spectrum induced by the irradiation is shown in orange color at the bottom.

[1] A. Fujishima *et al.*, J. Photochem. Photobio. C **1** (2000) 1.
[2] H. Onishi, ChemSusChem **12** (2019) 1825.
[3] Y. Uemura *et al.*, J. Phys. Chem. Lett. **13** (2022) 4207.

BL4B

Oxygen K-Edge XAS Study of $Eu_2Zr_2O_7$

S. Yoshioka[1], E. Kobayashi[2] and K. Oudaira[3]
[1]*Department of Applied Quantum Physics and Nuclear Engineering, Kyushu University, Fukuoka 819-0395, Japan*
[2]*Kyushu Synchrotron Light Research Center, Saga 841-0005, Japan*
[3]*Graduate school of Advanced Integration Science, Chiba University, Chiba 263-8522, Japan*

Rare earth zirconates ($Re_2Zr_2O_7$) such as $Eu_2Zr_2O_7$ and $Gd_2Zr_2O_7$ exhibit attractive potential as functional materials for thermal barrier coatings and nuclear fuel inert matrixes. $Re_2Zr_2O_7$ displays two types of crystal structures depending on the ionic radius ratio between Re and Zr. There are the pyrochlore structure and the oxygen deficient fluorite structure, with the former being considered a cation and oxygen vacancy ordered form of the latter. The transformation between pyrochlore and defective fluorite structures can be described as cationic disordering. Regrading the local coordination on the disordering, Re ions partly move from eight-coordinated site (CN8) to a six-coordinated site (CN6), whereas Zr ions partly move from CN6 to CN8. The structure changes related to the cationic disorder of pyrochlore under swift heavy ion (SHI) irradiation have been reported using diffraction techniques and transmission electron microscopy observations. X-ray absorption near edge structure (XANES) spectroscopy is a powerful method for structure characterization, providing information on local atomic coordination and electronic structures. Moreover, XANES offers a significant advantage for the elemental selectivity of the multi-cation compounds such as pyrochlore. In this study, we investigated oxygen local structure change in $Eu_2Zr_2O_7$ induced by SHI using X-ray absorption spectra (XAS).

Polycrystalline Eu_2Zr_2O samples were synthesized via a solid-state reaction. Stoichiometric amounts of Eu_2O_3 and ZrO_2 oxides were intimately mixed and pressed into disc at 100 MPa. Finally, the discs were sintered under air at 1500 °C using an electric furnace.

The sintered Eu_2Zr_2O sample was confirmed to have pyrochlore structure by X-ray diffraction (XRD). SHI irradiation experiments with 200 MeV Xe ions at fluences ranging from 5×10^{11} up to 1×10^{13} cm^{-2} were performed at the H1 beamline of the tandem ion accelerator facility in the Japan Atomic Energy Agency (JAEA)-Tokai.

O K-edge XANES measurements were performed on the BL4B beamline of UVSOR Okazaki, Japan, using the partial fluorescence yield (PFY) method. A varied-line-spacing plane gratings monochromator provided the O K-edge in the energy regions 520–560 eV. The samples were positioned with their surface perpendicular to the incident X-ray beam. Fluorescence X-rays of O K_α was collected using an energy dispersible silicon drift detector (SDD).

The O K-edge XANES spectra (at 525 eV) are shown in Fig. 1 for the Eu_2Zr_2O powder sample and reference bixbyite Eu_2O_3 and monoclinic ZrO_2 powder samples. The intensity of each spectrum was normalized to a value of 1 at 555 eV after the removal of the background intensity.

The spectrum shape of $Eu_2Zr_2O_7$ is clearly different from those of standard samples Eu_2O_3 and ZrO_2. The peaks A – C in the spectrum of Eu_2O_3 were assigned to transitions from the O 1s orbitals to unoccupied bands derived from the Eu 5d-π, 6p, 5d-σ orbitals, respectively [1].

Detailed analysis on the local environment of O in $Eu_2Zr_2O_7$ is in progress, employing a combined approach of XANES and first principles band structure calculations.

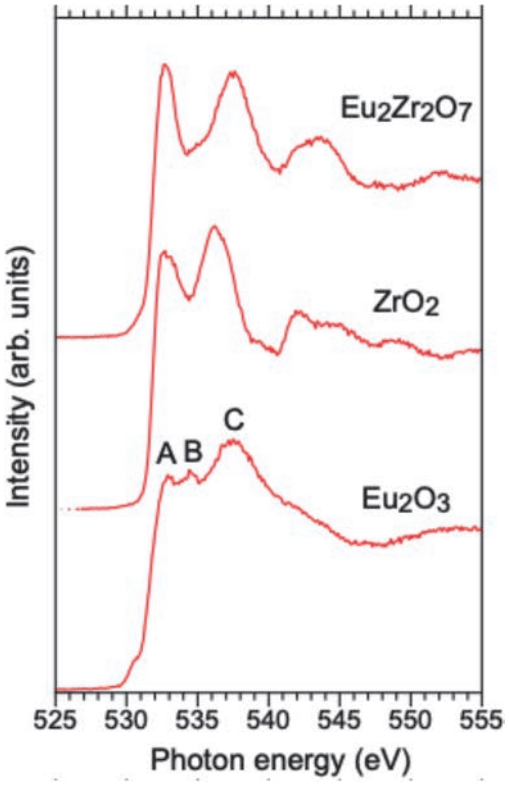

Fig. 1. O K-edge XANES spectra of pyrochlore Eu_2Zr_2O, including references spectra from bixbyite Eu_2O_3 and monoclinic ZrO_2 powder for comparison.

[1] A. B. Altman, *et al*., Dalton Trans. **45** (2016) 9948.

BL4B

Dissociation Following Double Auger Decay of Xenon Difluoride Molecules

Y. Hikosaka[1]
[1]*Institute of Liberal Arts and Sciences, University of Toyama, Toyama 930-0194, Japan*

Molecular inner-shell photoionization is usually followed by Auger decay, where occasionally two Auger electrons are emitted, resulting in the formation of triply-charged molecular ions. These ions are energetically unstable due to Coulomb repulsion among the three positive charges and typically fragment immediately after their formation. In this study, we employed multielectron-ion coincidence spectroscopy with a magnetic bottle electron spectrometer equipped with ion detection [1,2] to explore the dissociation of triply-charged states in xenon difluoride (XeF_2) [3], a molecule characterized by weak bonding between the central rare-gas atom and fluorine ligands.

The double Auger decay processes of the XeF_2 4d core-hole state can be isolated through electron triple coincidence which includes a 4d photoelectron. Figure 1 (top) displays the energy sum of the two other electrons detected in coincidence with a $4d_{3/2}$ photoelectron as a function of the XeF_2^{3+} binding energy, determined by the relationship: (XeF_2^{3+} binding energy) = ($4d_{3/2}^{-1}$ binding energy) − (sum of two Auger electrons' energy). The ratio of double to single Auger decay in the $4d_{3/2}^{-1}$ state is determined to be 33% ± 5%, considering electron detection efficiency. The XeF_2^{3+} spectrum generally shows a gradual rise from around 60 eV without distinct peaks. The triple ionization threshold is about 4 eV lower than that of atomic Xe. The observed triple ionization threshold for double Auger decay can be less than the vertical triple ionization energy. This discrepancy arises because the double Auger decay involves sequential processes that pass through the intermediate XeF_2^{2+} states, which lie below the vertical triple ionization energy. The second Auger steps originating from these XeF_2^{2+} states occur outside the Franck–Condon region of neutral ground state XeF_2.

Four ion species, Xe^{2+}, Xe^+, F^+, and XeF^{2+}, were detected in coincidence with the triple electrons including a $4d_{3/2}$ photoelectron. The dissociation pathways potentially forming these four ions are $Xe^{2+} + F^+ + F$, $Xe^+ + 2F^+$, and $XeF^{2+} + F^+$. To elucidate the contributions from these pathways, XeF_2^{3+} spectra filtered with these four ion species were obtained from fourfold coincidences between the three electrons and an ion. Figure 1 illustrates the coincidence spectra. The spectra corresponding to Xe^{2+}, Xe^+, and XeF^{2+} delineate the contributions from the dissociation pathways of $Xe^{2+} + F^+ + F$, $Xe^+ + 2F^+$, and $XeF^{2+} + F^+$, respectively. The spectrum coincident with F^+ includes contributions from all the dissociation pathways.

Dissociation to $XeF^{2+} + F^+$ occurs just above the triple ionization threshold and peaks around 60 eV. Dissociation to $Xe^+ + 2F^+$ begins around 62 eV and reaches its maximum near 68 eV. The onset of dissociation to $Xe^{2+} + F^+ + F$ is around 65 eV, with yield rapidly increasing as binding energy increases.

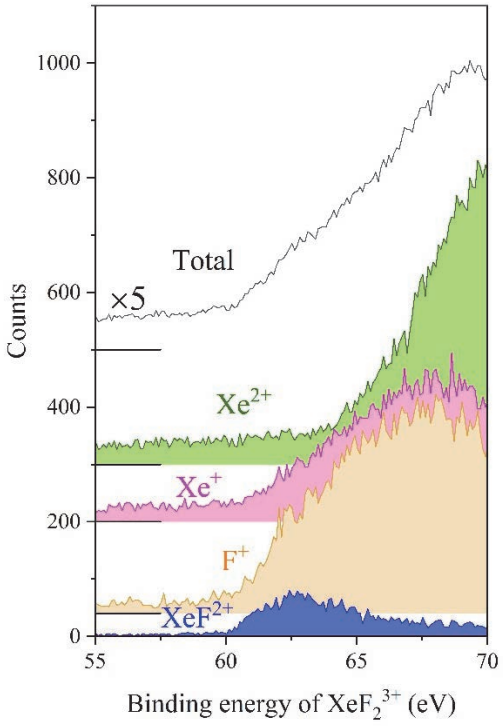

Fig. 1. Spectra of XeF_2^{3+} states selected by coincidence with fragment ions and the overall XeF_2^{3+} spectrum resulting from the $4d_{3/2}$ double Auger decay.

[1] Y. Hikosaka and E. Shigemasa, Int. J. Mass Spectrom. **439** (2019) 13.
[2] Y, Hikosaka, J. Electron Spectrosc. Relat. Phenom. **255** (2022) 147158.
[3] Y. Hikosaka, J. Chem. Phys. **160** (2024) 024304.

BL4B

X-ray Absorption Spectroscopy in Ferroelectric Nematic Liquid Crystals

F. Araoka[1], Y. Takanishi[2] and H. Iwayama[3]
[1]*RIKEN Center for Emergent Matter Science, Hirosawa 2-1, Wako, Saitama 351-0198, Japan*
[2]*Department of Physics, Kyoto Prefectural University of Medicine,1-5, Shimogamohangi-cho, Sakyo, Kyoto 606- 0823, Japan*
[3]*UVSOR Synchrotron Facility, Institute for Molecular Science, Okazaki 444-8585, Japan*

Ferroelectric nematics (NF) are a new group of polar fluid liquid crystals (LCs), wherein liquid-like fluidity and ferroelectricity co-exist. Such polar ordering was first predicted by the well-known physicist, Max Born, in the early 20th century. However, it had not been realized for a long time until its coincident discoveries in 2017 by two independent groups [1,2]. There are many fascinating physical properties of NF such as huge apparent permittivity values, large spontaneous polarization, strong nonlinear optical effects, and so on. Because of both scientific curiosity and vast potential for applications, it has attracted broad attention in the field of liquid crystal sciences.

Recently, we reported cybotactic cluster formation stabilizing the NF phase in diastereomeric DIO mixtures [3]. In this case, anisotropy of the smectic clusters, estimated from small/wide angle X-ray analysis, clearly shows growth of clusters as temperature decreases. This suggests a possibility that the side-by-side interaction may be an important role in stabilizing the polar ordering of the NF phase. Motivated by this, we have tackled resonant X-ray scattering to resolve polar distribution at the nanoscopic scale. However, due to strong absorption at the carbon K-edge, yet it is too difficult to detect a clear scattering pattern. Thus, we need to seek the possibility to use other resonant conditions in other elements, such as fluorine, or oxygen, which also takes a part of the molecular structure of the NF molecule.

In this study, we performed X-ray absorption spectroscopy for the NF liquid crystal, DIO-C3 (Fig. 1, left). The carbon, fluorine, and oxygen K-edge absorption spectra were taken by scanning the photon energy of the soft X-ray irradiated on the sample sandwiched between two silicon nitride (SiN) membrane films (Fig. 1). The sample film was heated by a hot stage which equips input/output window to allow the X-ray beam to pass through. The transmitted X-ray was detected by a photodiode instead of a cooled CCD used in the scattering experiment, and the generated photocurrent was recorded by a signal counter.

Plotted in Fig. 2 are typical carbon K-edge absorption spectra taken using the soft X-ray beam at BL3U. The spectra show two signature peak regions; one appearing in the lowest photon energy region (285~6 eV) is corresponding to the π-electrons in the molecule, the other in the higher energy region (above~286.5eV) to the α-electrons. Interestingly, the latter shows notable peak shift at the phase transition temperature between the nematic, antiferroelectric meso- and NF phases, while the former shows only scarce change either in the peak position or shape. This means, the head-to-tail dipolar interaction, which affects the longitudinal α-orbitals, is stronger than the effect of the side-by-side attraction contributed from the π-π interaction, in the present system. Thus, this is different from our expectation, described in the above introduction part. Based on this result, we further conducted K-edge absorption measurements for fluorene and oxygen by using the soft X-ray available at BL4B. The result will be discussed with a theoretically computed spectrum obtained with a density functional theory (DFT). Further calculation and analysis are currently on-going.

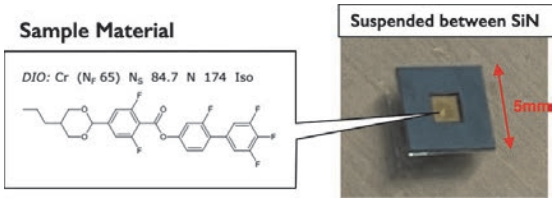

Fig. 1. Chemical structure of the NF molecule, DIO-C3 (Left), introduced between two SiN membrain films (Right).

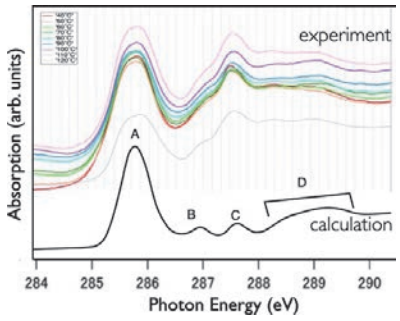

Fig. 2. Typical temperature-dependent absorption spectrum in the NF material, DIO-C3. The region A is corresponding to the π-orbital, and B, C and D are to the α-orbitals of alkyls and dioxanes.

[1] H. Nishikawa *et al.*, Adv. Mater. **29** (2017) 1702354.
[2] R. Mandle *et al.*, Chem. Eur. J. **23** (2017) 14554.
[3] H. Nishikawa *et al.*, Commun. Mater. **3** (2022) 89.

III-3

BL4B

Fragmentation Processes of 2-Iodothiophone in Doubly Charged States Studied by Multielectron-Ion Coincidence Spectroscopy

M. Fushitani[1], Y. Hikosaka[2], Y. Kimura[1] and A. Hishikawa[1,3]

[1]*Graduate School of Science, Nagoya University, Nagoya 464-8602, Japan*

[2]*Institute of Liberal Arts and Sciences, University of Toyama, Toyama 930-0194, Japan*

[3]*Research Center for Materials Science, Nagoya University, Nagoya 464-8602, Japan*

Breaking chemical bonds in a cyclic structure is an important step for ring-opening reactions. Among others, 2-iodothiophene (2-C_4H_3SI) is one of the prototype heterocyclic compounds which have been used to clarify the elementary processes in photoinduced ring-opening. Site-selective probing using ultrashort laser pulses in the extreme ultraviolet (EUV) and X-ray region is a promising method to directly capture details of the reaction [1, 2]. Such inner-shell probing often leads to the formation of highly charged states followed by ultrafast dissociation into different channels. Since the fragmentation pathways could be dependent on the initial geometry, it offers a unique approach to understand photoinduced processes in neutral states, including the ring-opening. Herein, we carried out multielectron-ion coincidence spectroscopy of I 4d inner-shell photoionization of 2-C_4H_3SI in the ground state to study the fragmentation processes after the core-hole decay.

Synchrotron radiation at 105 eV (single bunch mode) was used to ionize isolated 2-C_4H_3SI molecules and the produced electrons and ions were detected in coincidence by using a magnetic bottle type electron spectrometer with an ion-collecting electrodes [3,4].

The measured ion time-of-flight mass spectrum identifies formations of C_n (n = 1-4) hydrocarbons with a specific number of H atoms. Figure 1(a) shows I $4d_{5/2}$ Auger electron spectrum obtained in coincidence with I $4d_{5/2}$ photoelectrons and the parent 2-$C_4H_3SI^{2+}$ ions in the ground state while those with pairs of I^+ and the counterpart fragment ions are shown in Figs.1(b)-(i). All the Auger signals for the ion pairs appear in the lower energy region than the Auger peak at 33.1 eV of the parent 2-$C_4H_3SI^{2+}$, showing that these fragmentations take place mainly in electronically excited states in the doubly charged states. The Auger signals associated with the fragment ions can be classified into the 0-20 eV (Region I) and 20-32 eV (Region II) energy regions. It is found in Fig. 1(c) that $C_3H_3^+$ ions are selectively produced with I^+ ions in Region II while in Region I the fragment ions become C_3H^+ species instead of $C_3H_3^+$. On the other hand, C_4 and C_2 hydrocarbons in Figs. 1(b) and (d), appear as C_4H^+ and $C_2H_2^+$ ions, both of which are identified in Region I only. This suggests that a three-body fragmentation, 2-$C_4H_3SI^{2+} \rightarrow C_3H_3^+ + I^+ +$ CS, is a main channel to break the ring structure in Region II.

Auger signals for the fragment ions containing the S atom in Figs. 1(e)-(i), it turns out that $C_3H_3S^+$, C_2HS^+, CHS^+, and S^+ ions with a fixed number of H atoms are dominant products as the I^+ counterpart while for $C_4H_nS^+$ (n = 0-3) ions the number of the H atom depends on the Auger electron energies. It is noted that the Auger peak at 30.4 eV for the (I^+, $C_4H_3S^+$) ion in Fig. 1(e) exhibits much narrower spectral width compared to the other Auger peaks. This indicates that the $C_4H_3S^+$ moiety could keep its cyclic structure after the C-I bond fission, 2-$C_4H_3SI^{2+} \rightarrow C_4H_3S^+ + I^+$.

The present study reveals which electronic energy region of 2-$C_4H_3SI^{2+}$ preferentially produces specific fragment pair of ions with the characteristic numbers of C and H atoms, providing crucial information on the ring-opening processes.

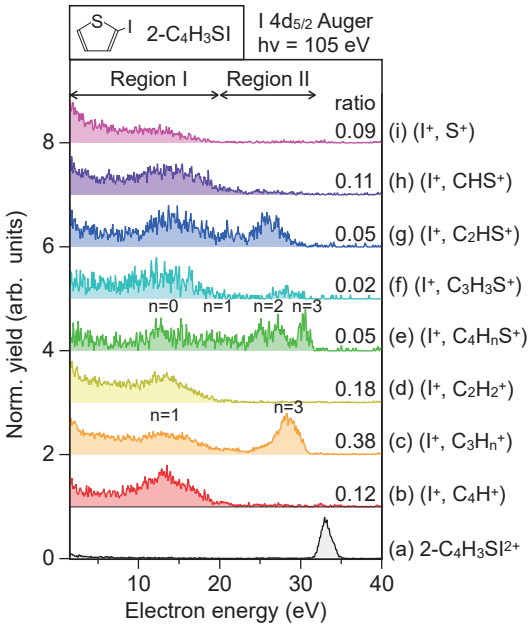

Fig. 1. Auger electron spectra of 2-iodothiophone by I $4d_{5/2}$ inner-shell photoionization at 105 eV, detected in coincidence with (a) 2-$C_4H_3SI^{2+}$, (b) (I^+, C_4H^+), (c) (I^+, $C_3H_n^+$(n = 1,3)), (d) (I^+, $C_2H_2^+$), (e) (I^+, $C_4H_nS^+$(n = 0-3)), (f) (I^+, $C_3H_3S^+$), (g) (I^+, C_2HS^+), (h) (I^+, CHS^+), and (i) (I^+, S^+) ions. The values for traces (b)-(i) represent the relative yield among these ion pairs.

[1] B. W. Toulson *et al.*, J. Chem. Phys. **159** (2023) 034304.

[2] W. O. Razmus *et al.*, Phys. Chem. Chem. Phys. **26** (2024) 12725.

[3] Y. Hikosaka, J. Electron Spectrosc. Rel. Phenom. **255** (2022) 147158.

[4] M. Fushitani *et al.*, J. Chem. Phys. **160** (2024) 174307.

BL4B

Coverage-Dependent Spin Reorientation Transition in Ni Thin Films on Cu(001) Induced by Pd Overlayers

T. Miyamachi[1,2], N. Okamura[1], A. Iwai[1], H. Ono[1], N. Maejima[3,4], O. Ishiyama[3,4], E. Nakamura[5], H. Iwayama[5], T. Yokoyama[3,4] and M. Mizuguchi[1,2]

[1]*Department of Materials Science and Engineering, Nagoya University, Nagoya 464-8603, Japan.*
[2]*Institute of Materials and Systems for Sustainability (IMaSS), Nagoya University, Nagoya 464-8601, Japan.*
[3]*Institute for Molecular Science, Myodaiji-cho, Okazaki 444-8585, Japan*
[4]*The Graduate University for Advanced Studies, Myodaiji-cho, Okazaki 444-8585, Japan*
[5]*UVSOR Synchrotron Facility, Institute for Molecular Science, Okazaki 444-8585, Japan*

Thin film heterostructures have been widely studied because of novel phenomena developed by the formation of the heterointerface. Especially for the heterostructure composed of magnetic materials, interface conditions such as lattice strain, mixing drastically change magnetic properties of the whole system [1]. In this study, we fabricate Pd/Ni thin film heterostructures on Cu(001) and investigate their structural, electronic, and magnetic properties by low energy electron diffraction (LEED) and x-ray absorption spectroscopy/magnetic circular dichroism (XAS/XMCD). Ni thin films grown on Cu(001) are known to exhibit the spin reorientation transition (SRT) from in-plane magnetization to out-of-plane magnetization with increasing the coverage [2]. Since the SRT is associated with changes in the lattice constant near surface, adding Pd overlayers with significantly larger lattice constant than Ni can modify magnetic properties of Ni thin films by the formation of Pd/Ni heterointerface.

To fabricate Pd/Ni thin film heterostructures, we grow 6 and 12 monolayer (ML) Ni thin films on Cu(001) at room temperature. Then, 2, 6 and 12 MLs of Pd overlayers are grown onto each Ni thin film. LEED patterns of Pd/Ni thin-film heterostructures reveal that both Ni and Pd layers grow epitaxially on Cu(001) but the surface lattice constant of Ni expands by adding Pd overlayers. To investigate electronic, and magnetic properties of Pd/Ni thin film heterostructures, XAS/XMCD measurements are performed at BL4B in UVSOR by total electron yield mode at B = 0 - ± 5 T and T = 6.6 K. The XMCD spectra are obtained at the normal (NI: θ = 0°) and the grazing (GI: θ = 55°) geometries by detecting $\mu_+ - \mu_-$, where μ_+ (μ_-) denotes the XAS recorded at Ni and Pd L adsorption edges with the photon helicity parallel (antiparallel) to the sample magnetization. Note that θ is the angle between the sample normal and the incident x-ray. Element specific magnetization curves of Ni layers are also recorded by plotting the Ni XAS L_3 peak intensity normalized by L_2 one as a function of the magnetic field. The deposition rates and coverages of Ni and Pd layers are crosschecked by the quartz-crystal microbalance (QCM) and XAS edge jumps at L-edges of Ni and Pd relative to of Cu L-edge [3].

We first investigate magnetic properties of bare Ni thin films on Cu(001) by XAS/XMCD. Comparing XAS/XMCD spectra recorded in the NI and GI geometries, we reveal that 6 ML Ni thin films show strong in-plane magnetization the easy magnetization direction of 12 ML Ni thins film is slightly toward the out-of-plane direction, which is in good agreement with previous work investigated by ferromagnetic resonance measurements [2].We find from Pd coverage dependence of Ni magnetization curve that adding Pd overlayer modifies the magnetic anisotropy of Ni thin films. For 12 ML Ni thin films, the easy magnetization direction gradually shifts from out-of-plane to in-plane direction with increasing Pd coverage. On the other hand, adding Pd overlayer further stabilizes the in-plane magnetization of 6 ML Ni films. Interestingly, the stabilization of the in-plane magnetization is completed when 2 MLs of Pd are deposited no further changes are recognizable with increasing Pd coverage. The results indicate that the degree of lattice strain of Ni induced by Pd overlayers and the hybridization strength at the Pd/Ni heterointerface, which both modify the magnetic anisotropy of Ni thin film, are strongly dependent on Ni coverage.

[1] S. Nakashima *et al*., Adv. Funct. Mater. **29** (2019) 1804594.
[2] B. Schulz *et al*., Phys. Rev. B **50** (1994) 13467.
[3] H. Ono *et al*., J. Phys. Chem. C **127** (2023) 23935.

BL4B

Spin Reorientation Transition of Co Nano Islands by the Formation of Organic-Inorganic Hybrid Interface

T. Miyamachi[1,2], H. Ono[1], K. Fujimoto[1], K. Yoshida[1], N. Maejima[3,4], O. Ishiyama[3,4], E. Nakamura[5], H. Iwayama[5], T. Yokoyama[3,4] and M. Mizuguchi[1,2]

[1]*Department of Materials Science and Engineering, Nagoya University, Nagoya 464-8603, Japan.*
[2]*Institute of Materials and Systems for Sustainability (IMaSS), Nagoya University, Nagoya 464-8601, Japan.*
[3]*Institute for Molecular Science, Myodaiji-cho, Okazaki 444-8585, Japan*
[4]*The Graduate University for Advanced Studies, Myodaiji-cho, Okazaki 444-8585, Japan*
[5]*UVSOR Synchrotron Facility, Institute for Molecular Science, Okazaki 444-8585, Japan*

An organic-inorganic hybrid interface has attracted attention due to its controllable interface electronic state by the proper choice of organic and inorganic materials. Especially for the system composed of organic molecules and an inorganic magnetic material, a variety of novel spin functionalities with the help of long spin diffusion length of organic molecule can emerge via the magnetic interaction at the organic-inorganic interface. Since the degree of the magnetic interaction strongly replies on the spin polarization of the inorganic magnetic material near the Fermi energy, element specific investigations of the organic-inorganic hybrid interface are important to understand the impact of the formation of the organic-inorganic hybrid interface on the magnetic properties of the inorganic magnetic material. In this work, we fabricate the organic-inorganic hybrid interface composed of [1,2,5] Thiadiazolo [3,4-f][1,10]phenanthroline 1,1-dioxide ($tdapO_2$) and Co nano island and investigate its electronic/magnetic properties element specifically by x-ray absorption spectroscopy/x-ray magnetic circular dichroism (XAS/XMCD).

XAS/XMCD measurements are conducted at BL4B in UVSOR by total electron yield mode at B = 0 - ± 5 T and T = 7.7 K. The XMCD spectra are obtained at the normal (NI: θ = 0°) and the grazing (GI: θ = 55°) geometries by detecting $\mu_+ - \mu_-$, where μ_+ (μ_-) denotes the XAS recorded at Co L adsorption edges with the photon helicity parallel (antiparallel) to the sample magnetization. Note that θ is the angle between the sample normal and the incident x-ray. Magnetization curves of Co nano islands are recorded by plotting the L_3/L_2 Co XAS peak intensity as a function of the magnetic field.

Co islands are first grown by deposition of 0.4 monolayer Co onto Cu(111) at room temperature. We investigate the morphology of Co islands by scanning tunneling microscopy (STM) in advance, and confirm the formation of isolated bilayer Co nano islands at Co coverage of 0.4 monolayer. The deposition rate of Co is evaluated by the quartz-crystal microbalance (QCM) and XAS edge jump [1]. Then, $tdapO_2$ molecules are sublimated by heating at 380 K and deposited onto Co islands. The deposition amount of $tdapO_2$ is evaluated by QCM and set to several molecular layers in this study.

In XAS/XMCD measurements, we focus on the remanent magnetization and coercivity in the Co magnetization curve. While the Co magnetization curve recorded in the GI geometry shows a clear hysteresis loop, reduced remanent magnetization and a smaller hysteresis loop are observed for that recorded in the NI geometry. The results reveal in-plane magnetic easy axis of Co nano islands, which is consistent with previous study [2]. After the deposition of $tdapO_2$, significant changes are observed for Co magnetization curve recorded in the NI geometry. We find that the remanent magnetization increases by a factor of two, and the coercivity by a factor of seven, which induces the spin reorientation transition (SRT) of Co nano islands from in-plane direction to out-of-plane direction. These results indicate that substantial enhancement of perpendicular magnetic anisotropy of Co nano island is caused by the interface formation with $tdapO_2$. In future work, we will investigate the adsorption geometry and electronic structures of $tdapO_2$ molecules by STM and discuss the origin of the SRT of Co nano islands.

[1] H. Ono *et al*., J. Phys. Chem. C **127** (2023) 23935.
[2] M. Zhang *et al*., J. Phys.: Condens. Matter **12** (2000) 783.

Angle-Resolved Photoemission Circular Dichroism for Chiral Molecule Overlayer on Monolayer WS_2

F. Nishino[1,2], K. Fukutani[1,2], P. I. Jaseela[1,2], J. Brandhoff[3], F. Otto[3], M. Grünewald[3], M. Schaal[3], J. Picker[4], Z. Zhang[5], A. Turchanin[4], S. Makita[6], H. Iwayama[6], T. Hirose[5], T. Fritz[3] and S. Kera[1,2,6]

[1]*Institute for Molecular Science, Okazaki 444-8585, Japan*
[2]*School of Physical Sciences, The Graduate University for Advanced Studies, Okazaki 444-8585, Japan*
[3]*Institute of Solid State Physics, Friedrich Schiller University Jena, Helmholtzweg 5, 07743 Jena, Germany*
[4]*Institute of Physical Chemistry, Friedrich Schiller University Jena, Lessingstraße 10, 07743 Jena, Germany*
[5]*Institute for Chemical Research, Kyoto University, Gokasho, Uji, Kyoto 611-0011, Japan*
[6]*UVSOR Synchrotron Facility, Institute for Molecular Science, Okazaki 444-8585, Japan*

A chirality-induced spin selectivity (CISS) effect with controlled chiral molecules on various solid surfaces has been actively studied for various applications, such as for spintronics and enantio-separations [1]. On the other hand, many aspects of this phenomenon, including its mechanism underlying its extraordinarily large spin polarization effects, remain unknown.

Our approach to this challenge is to fabricate well-defined chiral molecular systems on solid surfaces with known spin-polarized electronic band structures, and to investigate how the surface chirality affects the emitted electrons from the solid by angle-resolved photoemission spectroscopy (ARPES).

As a preliminary study, in this work, we used angle-resolved photoemission circular dichroism (CD-ARPES) for the system of chiral molecular overlayer on achiral substrate possessing fully spin-polarized electrons to assess how the electrons emitted from the substrate recognize the surface chirality.

The enantiopure chiral molecule, thiadiazole-[9] helicene (TD[9]H) [2], was used in this study as show in Fig. 1(a). The substrate used was a monolayer WS_2/Au(111) (ML-WS_2) with fully spin-polarized bands at $\overline{K}$' and $\overline{K}$ points [3]. After depositing the enantiopure TD[9]H on the ML-WS_2 under ultra-high vacuum condition, low-energy electron diffraction (LEED) showed an ordered molecular overlayer with broken mirror-symmetry, indicating the surface chirality has been induced on the system.

Following the confirmation of the surface chirality, CD-ARPES measurements were performed, using left circularly polarized (LCP) and right circularly polarized (RCP) lights for both the clean substrate and the (*M*)-TD[9]H/ML-WS_2 samples, as shown in Fig. 1(b).

Figures 1(c)-(e) show the CD-ARPES maps obtained for clean ML-WS_2 substrate. It can be seen that the dichroic signals at the $\overline{\Gamma}$-$\overline{M}$ plane [black dotted lines in Figs. 1(c), 1(d) and the entire map in Fig. 1(e)], which is the mirror plane of the substrate, is very weak. Furthermore, the dichroic signals in the $\overline{\Gamma}$-$\overline{K}$ and $\overline{\Gamma}$-$\overline{K}$' directions are seen to be generally anti-symmetric with respect to the $\overline{\Gamma}$-$\overline{M}$ plane.

These characteristics of dichroic signals from

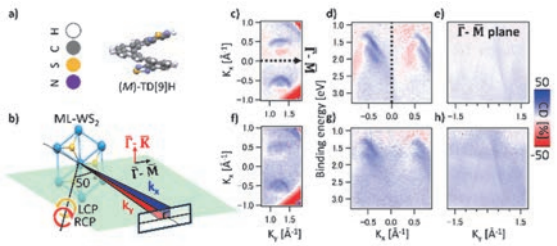

Fig. 1. (a) Molecular structures of (*M*)-TD[9]H. (b) Schematic illustration of CD-ARPES setup. The relative orientations of the sample and the photoelectron analyzer slit are shown. (c)-(e) CD-ARPES map of ML-WS_2. (f)-(h) CD-ARPES map of (*M*)-TD[9]H/ML-WS_2. (c) and (f) shows constant-energy cut and (d), (g) is the intensity plots in E-k_x slice. (e) and (h) is the intensity plots in E-k_y slice.

substrate can readily be understood from the point of view of symmetry. Since the substrate is achiral and the mirror plane of the crystal coincides with the plane of light incidence, it must hold that $I_{RCP}(k_x, k_y) = I_{LCP}(-k_x, k_y)$ (Equation 1), where I_{RCP} and I_{LCP} are the photoelectron intensities with RCP and LCP lights, respectively. That is, the achirality of substrate is reflected in our CD-ARPES results.

Next, the CD-ARPES results after the deposition of (*M*)-TD[9]H are shown in Figs. 1(f)-(h). Unlike the CD-ARPES results from the clean substrate, finite (blue) dichroic signals were observed uniformly in the substrate bands, molecular orbitals and inelastic scattering regions even in the E-k slice of the $\overline{\Gamma}$-$\overline{M}$ plane as can be seen in Fig. 1(h). While more investigations are necessary, the apparent violation of equation 1 above could arise from the loss of achirality (i.e., emergence of chirality) for the electrons in the system of chiral molecular overlayer on achiral substrate.

[1] S.-H. Yang *et al*., Nat. Rev. Phys. **3** (2021) 328.
[2] Z. Zhang *et al*., Tetrahedron **142** (2023) 133514.
[3] P. Eickholt *et al*., Phys. Rev. Lett. **121** (2018) 136402.

BL4B

Development of XANES Imaging Method for Visualizing Intracellular Chemical Species

R. Sasaba[1,2] and H. Iwayama[2]
[1]*Graduate School of Frontier Biosciences, The University of Osaka, Suita 565-0871, Japan*
[2]*UVSOR Synchrotron Facility, Institute for Molecular Science, Okazaki 444-8585, Japan*

Detecting the distribution of intracellular molecules or chemical components is very important. Several imaging methods to visualize them, such as Raman microscopy, have been proposed so far. Since the spectral structures of X-ray Absorption Near Edge Structure (XANES) spectroscopy depend on the chemical species, we are developing a XANES imaging method to visualize the distribution of chemical species within a cell using contact-type soft X-ray microscopy [1].

In this method, we measure transmitted X-ray images of biological samples at K- or L-edge energies of elements such as carbon, sulfur, and iron. Biological samples are placed on a Ce:YAG scintillator and covered with a 100 nm-thick Si_3N_4 membrane. The transmitted X-ray image is converted into a visible light image by the scintillator, and then captured by a CMOS camera. By changing photon energies, we can obtain photon-energy dependence of transmitted images Is(X, Y, E), where X and Y represent the positions of the camera and E is a photon energy, respectively. We also measure blank data I_0(X, Y, E) without the sample. From the Lambert-Beer law, we can obtain a three-dimensional XANES image (X, Y, E) from I_0(X, Y, E) and Is(X, Y, E).

The experiment was performed on the beamline BL4B at UVSOR-III. Figure 1 shows the observation result of a human oral epithelial cell using our contact-type soft X-ray microscopy and XANES spectra at four different positions (X,Y) on the sample. Each of the four XANES spectra is different. The No. 1 XANES spectrum corresponds to a cell-free region and consistently shows values close to zero, indicating the background of the spectroscopy. The No. 2 spectrum corresponds to the edge of a cell and exhibits a strong peak around 287 eV. The No. 3 spectrum, taken from the inner region of the cell, shows two peaks at approximately 285 eV and 287 eV. The No. 4 spectrum, acquired from the center of the cell, also exhibits two peaks; however, their intensities are significantly different.

After normalizing all XANES spectra, we extract some feature values from XANES spectra using machine learning techniques. Figure 2 shows the results of these feature calculations. Figure 2(a) displays the peak area around 285 eV, which reflects the amount of aromatic compounds. Figure 2(b) shows the peak area around 287 eV, corresponding to alkyl groups. Figure 2(c) represents the ratio between the peaks at 285 eV and 287 eV, providing contrast related to the relative abundance of aromatic and alkyl compounds. Figure 2(d) shows the spectral difference around 295-320 eV.

These visualized features help us to distinguish different regions within the cell based on their chemical compositions. For example, we could now know how aromatic compounds distribute within a cell.

We are currently working on applying this method to various types of biological samples, such as MDCK cells.

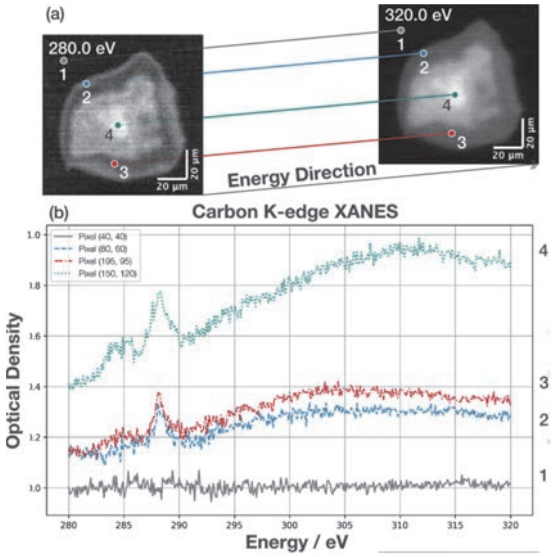

Fig. 1. The imaging result of a human oral epithelial cell using contact-type soft X-ray microscopy and XANES spectra at four different pixels.

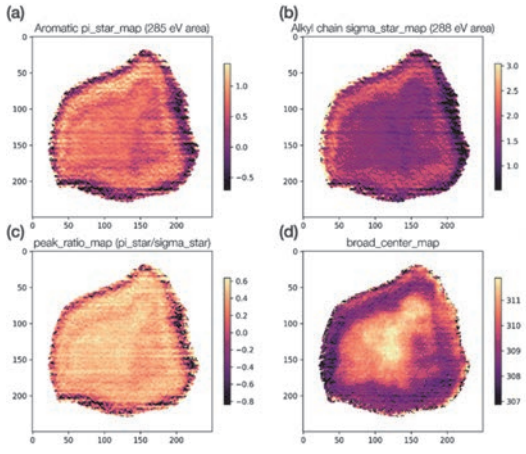

Fig. 2. Maps of spectral features calculated from individual XANES spectra at each pixel position.

[1] T. Ejima *et al.*, J. Phys.: Conf. Ser. **463** (2013) 1.